Supporting Information for

Self-assembly behavior of Phenanthroimidazole and Naphthalene Pendant Photoluminescent Ionic Liquid and its implication towards cascade Detection Hg^{2+} and I^- ions

Najmin Tohora and Sudhir Kumar Das*

Department of Chemistry, University of North Bengal, Raja Rammohunpur, Darjeeling,

West Bengal-734013, India

Corresponding author: (Dr. S. K. Das; E-mail: sudhirkumardas@nbu.ac.in)

S1. Experimental sections

S1.1 General Method & Instrumentations

Chemical reagents are purchased from Sigma Aldrich, India, and used without further purification. Anhydrous solvents and HPLC spectroscopic grade were obtained from Merck, India. 9, 10-phenanthrenequinone, 1-naphthaldehyde and trihexyltetradecylphosphonium chloride ([TTP]Cl) are purchased from Sigma-Aldrich, India. All the metal salts, anions, and biologically relevant molecules used in the present study are purchased from Sigma-Aldrich (India) and TCI (India), respectively. Dimethyl sulphoxide (DMSO-d_6) is obtained from Sigma-Aldrich, India, and used for NMR spectral analysis. Quatro Micro API (MICROMASS, UK), lc-WATERS 2695 spectrometer having detector PDA2998, ESI_Negative with capillary voltage 3 kV, Cone -30 V and extractor-3 V employing source and dissolving temperature -90℃ and -250℃ respectively using dissolving gas-450 Litre/hour with flow rate-10 μL/min. UV-visible spectral studies are carried out on a HITACHI U-2910, and fluorescence experiments are carried out on a HITACHI F-7100 fluorimeter with a 5 nm excitation and emission slit, respectively. Throughout the steady-state emission experiment, excitation and emission wavelengths are maintained at 370 nm and 390-720 nm, respectively.

The size and shape of the **nBTNP** are estimated by field emission scanning electron microscopy (SEM) (ZEISS) employing an operating voltage of 50 kV by drop casting the required amounts of **nBTNP** on the carbon-coated copper grids. The average particle size is determined by considering the size of more than 100 particles. The hydrodynamic radius of **nBTNP** is measured employing the dynamic light scattering (DLS) technique (Anton Paar Litesizer 500). The zeta potential (ζ) of nanoparticles is also obtained by this instrument using a capillary ζ-cell.

S1.2 General procedure for UV-visible and fluorescence experiments

The stock solutions of the sensor (23 μM), metal chloride solutions (1.2×10^{-3} M), and the sodium & potassium salts of the anions (1.2×10^{-3} M) were prepared in aqueous solution. The fluorescence response of various anions (ClO_4^-, F^-, BPh_4^-, SO_4^{2-}, I^-, Cl^-, Br^-, CO_3^{2-}, PO_4^{3-}) and metal ions (Al^{3+}, Ba^{2+}, Ca^{2+}, Cu^{2+}, K^+, Mn^{2+}, Na^+, Ni^{2+}, Pb^{2+}, Sn^{2+}, Zn^{2+}) were investigated. The probe's selectivity has been tested for all metal ions and anions using fluorescence experiments. To 2 mL of the sensor, 33 μM of each metal ion solution was added and stirred before fluorescence measurements. The fluorescence and UV–visible titrations were performed using varying concentrations of metal ions and anion solutions.

S1.3 Measurement of fluorescence quantum yield

For the estimation of fluorescence quantum yield, we have considered the quinine sulfate as a standard in 1(N) H_2SO_4 (Φ=0.546) [1]. Using the equation $: \Phi = \Phi_s\left(\frac{F_x}{F_s}\right)\left(\frac{A_s}{A_x}\right)\left(\frac{{\eta_x}^2}{{\eta_s}^2}\right)$, where Φ stands for quantum yield, F is the integrated fluorescence intensity, A is the absorbance, η defines the refractive index of the solvent, subscript ‘s’ defines the standard quinine sulfate, and x is the unknown one, we have calculated the quantum yield (Φ) of the nano-optode **nBTNP** and **nBTNP** with Hg^{2+}.

Characterization of compound C: (^{1}H NMR, DMSO-d_6, 400 MHz, in ppm units): 11.93 (s, 1H, NH), 8.93 (d, 2H), 8.55 (d, 1H), 8.12 (d, 2H), 8.08 (d, 1H), 8.04 (d, 1H), 7.95 (d, 1H), 7.88 (dd, 2H), 7.82 (dd, 2H), 7.61 (dd, 1H), 7.55 (d, 2H) (**Fig. S1**).

Characterization of compound D: (^{1}H NMR, DMSO-d_6, 400 MHz, in ppm units): 8.90 (d, 2H), 8.38 (d, 1H), 8.32 (d, 1H), 8.10 (d, 2H), 8.08 (d, 1H), 7.93 (d, 1H), 7.9 (dd, 2H), 7.8 (dd, 2H), 7.79 (dd, 1H), 7.55 (d, 2H) (**Fig. S3**).

Characterization of BTNP: (^{1}H NMR, DMSO-d_6, 400 MHz, in ppm units): 8.90 (d, 2H), 8.38 (d, 1H), 8.32 (d, 1H), 8.1 (d, 2H), 8.08 (d, 1H), 7.93 (d, 1H), 7.90 (dd, 2H), 7.80 (dd,

2H), 7.79 (dd, 1H), 7.55 (d, 2H), 2.22-0.88 (various m, 68 H) (**Fig. S5**). **^{31}P NMR** (400 MHz, DMSO-d_6, δ (ppm): 33.93 (**Fig. S8**).

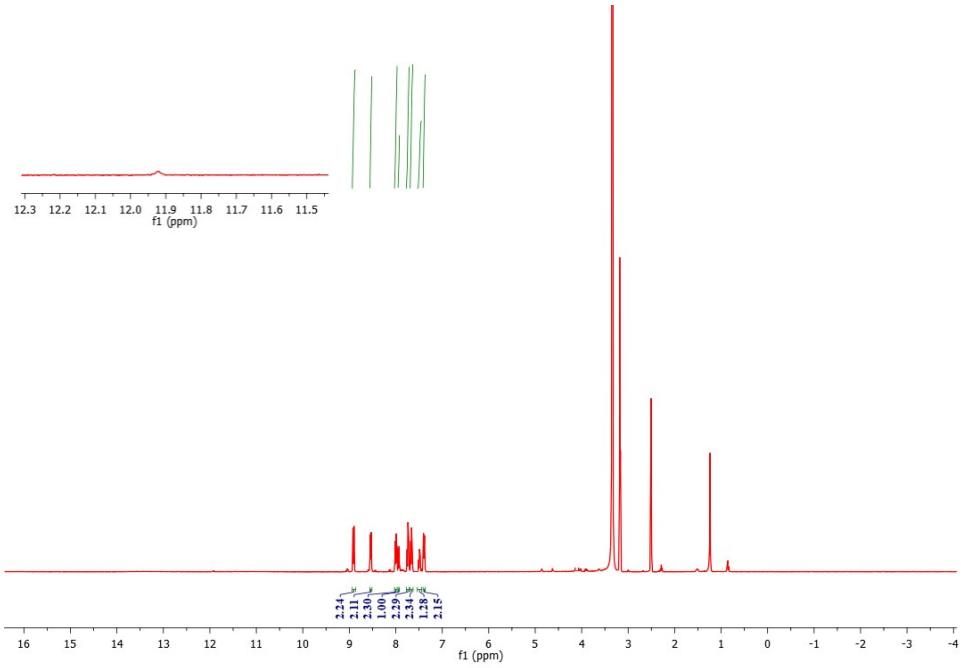

Fig. S1: ^{1}H NMR spectrum (DMSO-d_6, 400 MHz) of compound C.

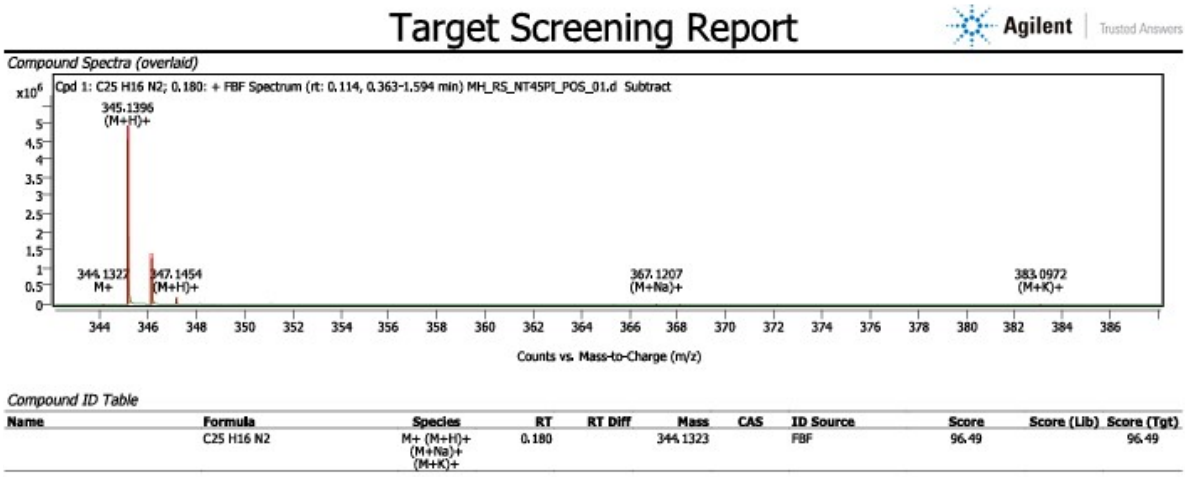

Fig. S2: HRMS spectra of compound C.

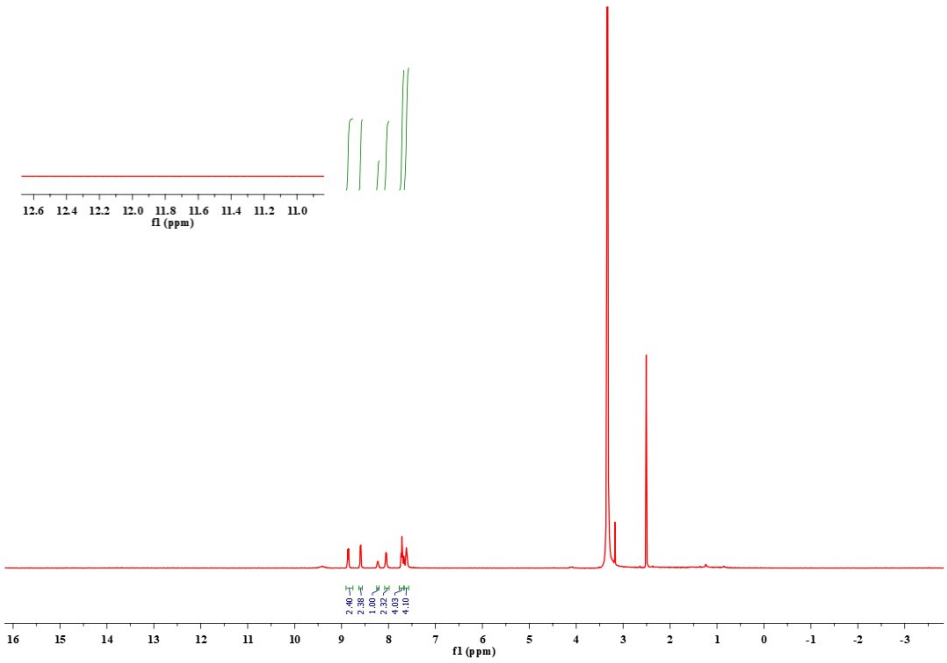

Fig. S3: ^{1}H NMR spectrum (DMSO-d_6, 400 MHz) of compound D.

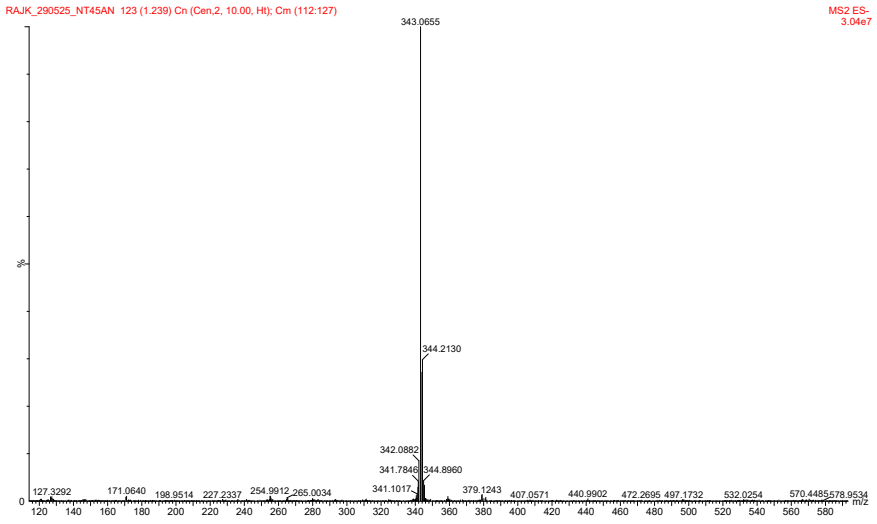

Fig. S4: LC-MS spectra of the negative component of compound D.

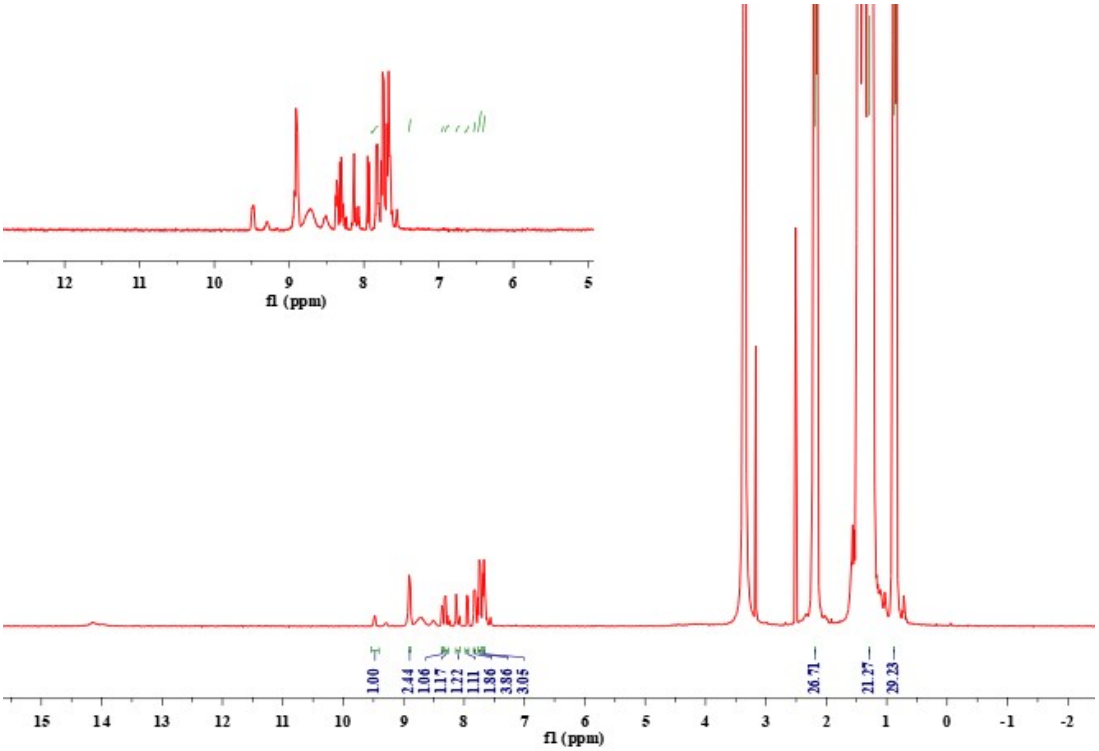

Fig. S5: ^{1}H NMR spectrum (DMSO-d_6, 400 MHz) of **BTNP**.

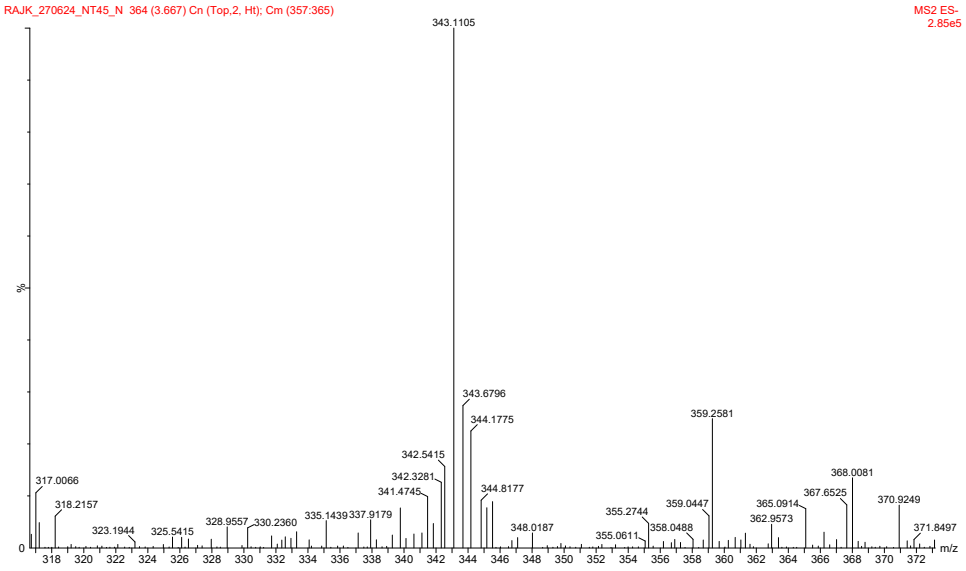

Fig. S6: LC-MS spectra of the negative component of **BTNP**.

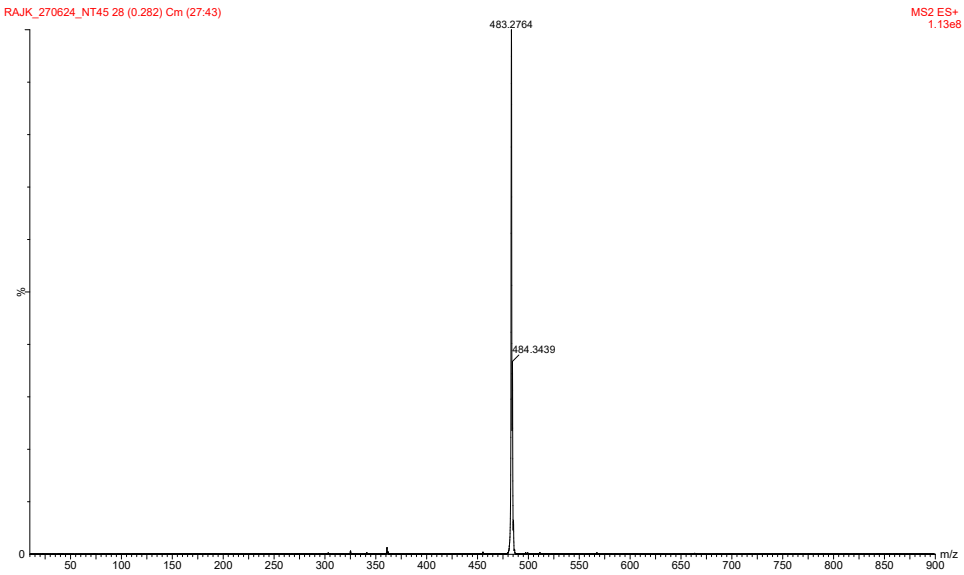

Fig. S7: LC-MS spectra of the positive component of **BTNP**.

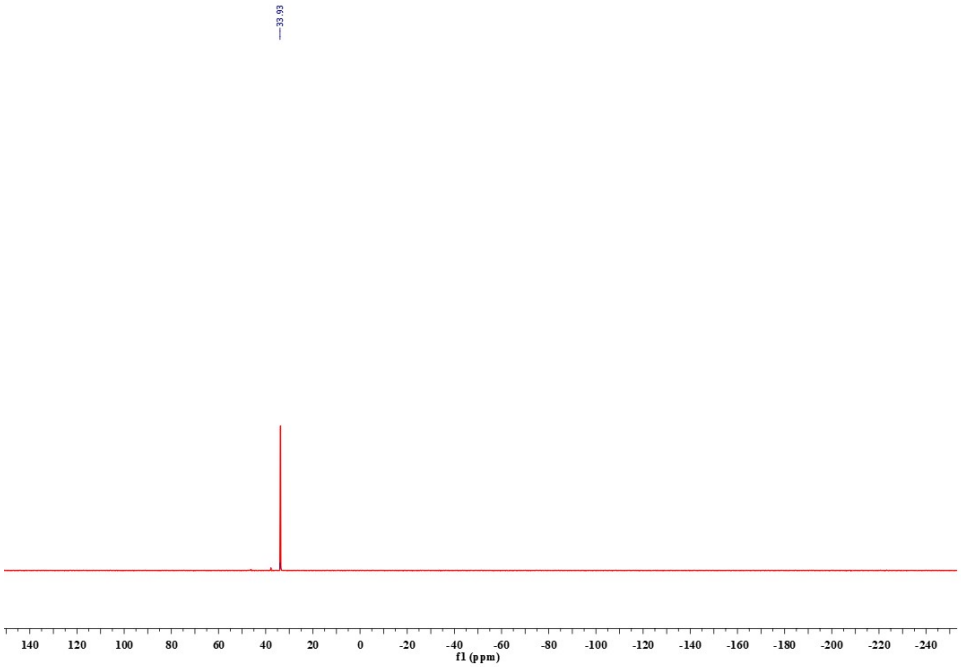

Fig. S8: ^{31}P NMR spectrum (DMSO-d_6, 400 MHz) of **BTNP**.

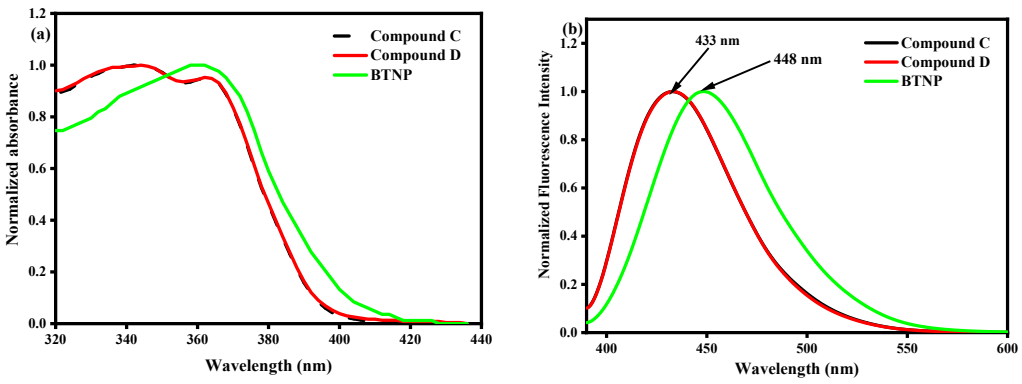

Fig. S9: (a) The normalized absorption spectra of compound C, D, and **BTNP** in DMSO. **(b)** The normalized fluorescence spectra of compounds C, D, and **BTNP** in DMSO.

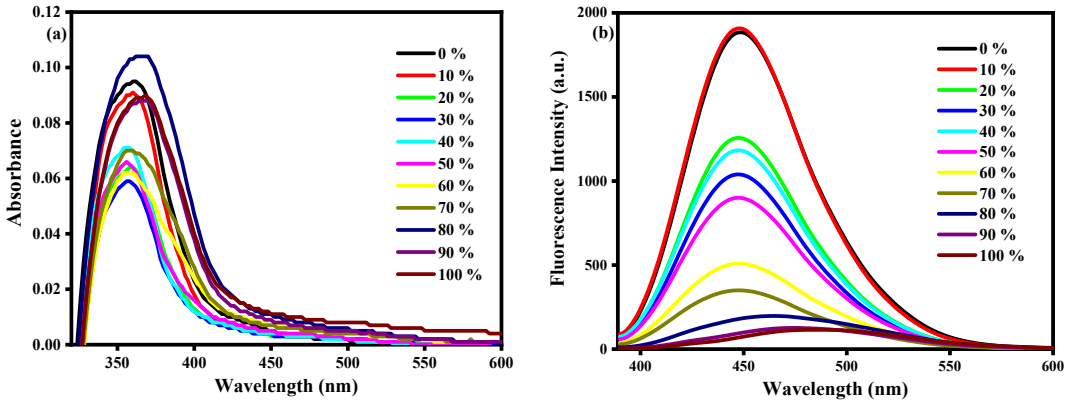

Fig. S10: (a) UV-vis absorption spectra of **BTNP** in different percentages of water. **(b)** Fluorescence spectra of **BTNP** in water-DMSO mixed solvents demonstrating ACQ.

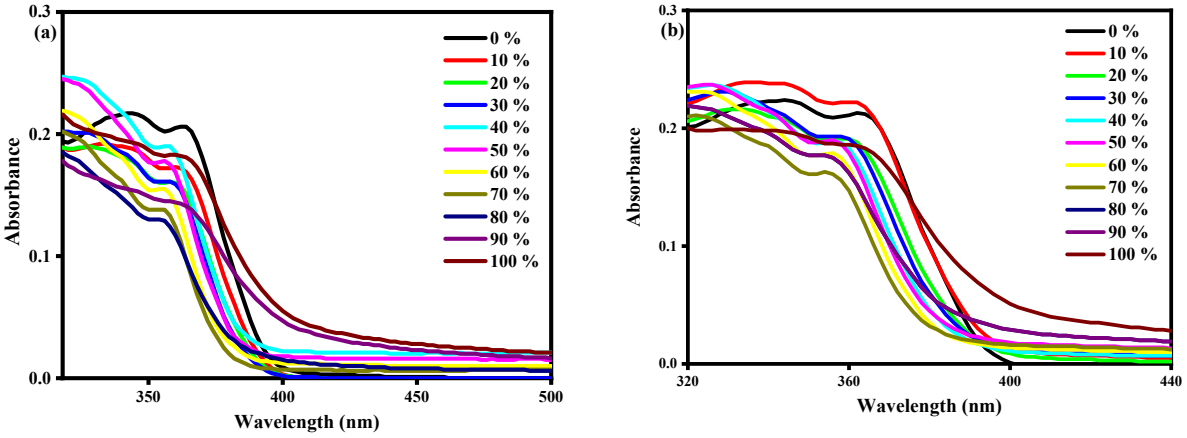

Fig. S11: (a) UV-vis absorption spectra of Compound C in different percentages of water. **(b)** UV-vis absorption spectra of Compound D in different percentages of water.

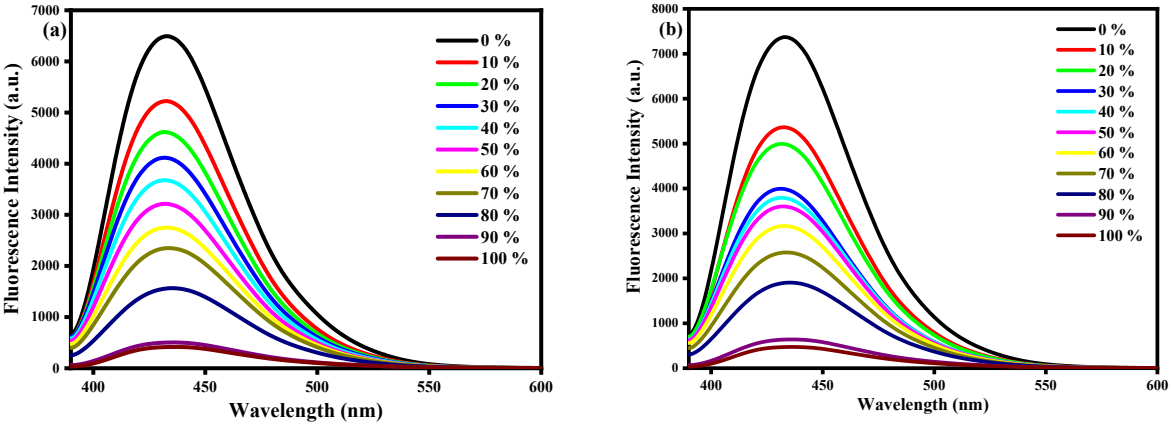

Fig. S12: (a) Fluorescence spectra of Compound C in water-DMSO mixed solvents. **(b)** Fluorescence spectra of Compound D in water-DMSO mixed solvents.

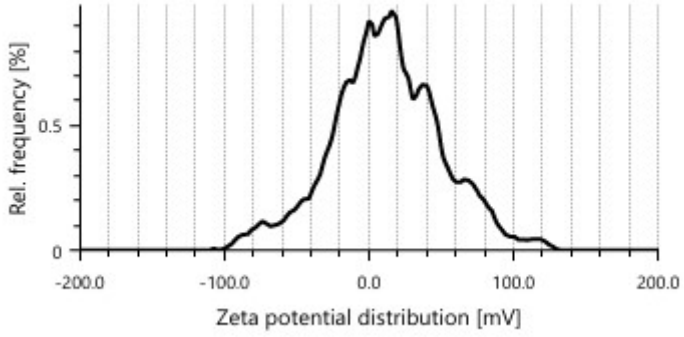

Fig. S13: The relative frequency vs. zeta potential distribution curve for the determination of the zeta potential of **nBTNP**.

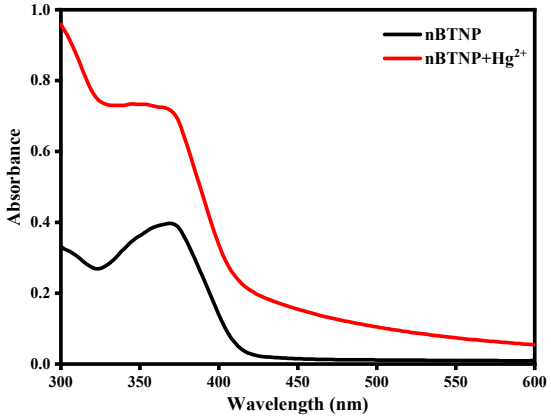

Fig. S14: UV-visible absorption spectra of **nBTNP** and **nBTNP**+Hg^{2+}.

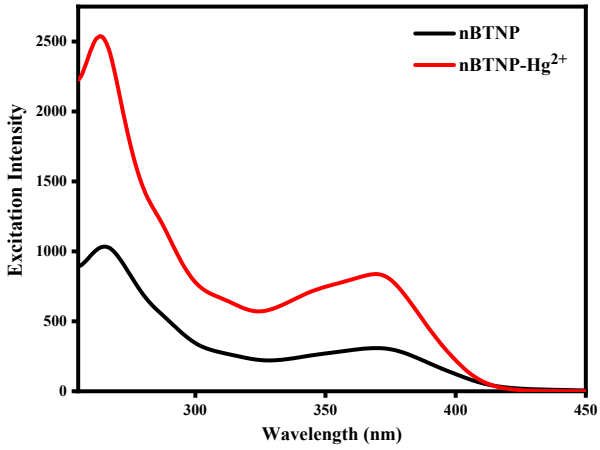

Fig. S15: The excitation spectra of **nBTNP** and **nBTNP**-Hg^{2+}.

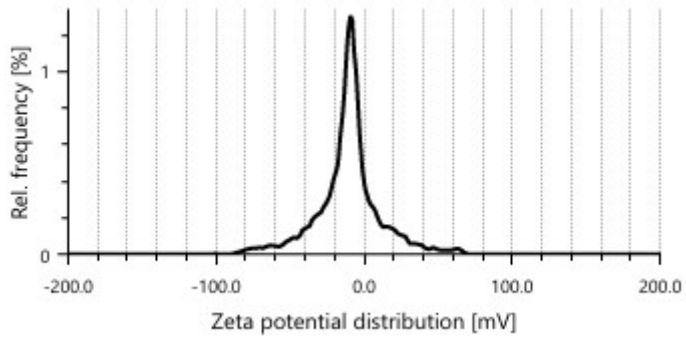

Fig. S16: The relative frequency vs. zeta potential distribution curve for the determination of the zeta potential of the **nBTNP-Hg^{2+}** system.

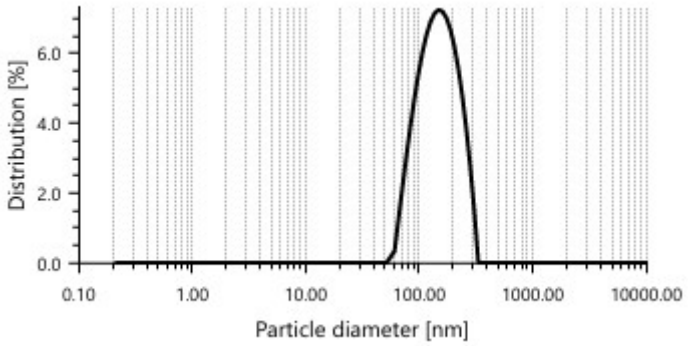

Fig. S17: DLS analysis showing the size distribution of the **nBTNP**-Hg^{2+} system**.**

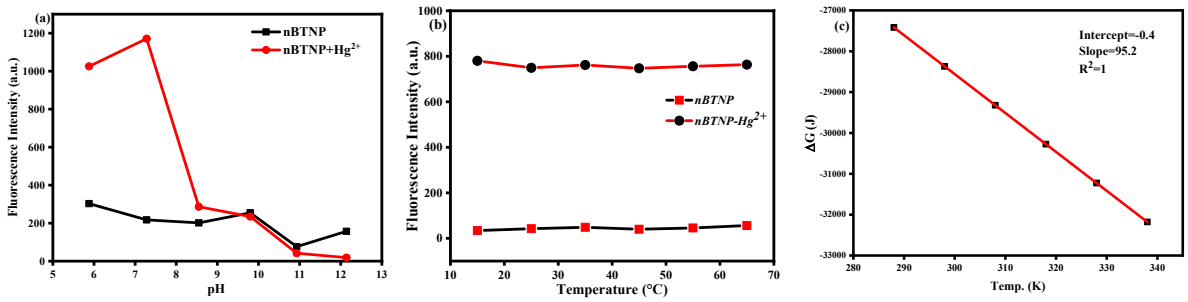

Fig. S18: (a) The impact of pH on photoluminosity of **nBTNP** with and without Hg^{2+} at 25 ^{o}C. **(b)** Temperature-dependent fluorescence study of **nBTNP** and **nBTNP**-Hg^{2+} complex. **(c)** The linear calibration curve for calculating the ΔH and ΔS values.

Table S1. Absorption spectra in the UV-visible range and photoluminescence data of compound C were measured in different media and expressed in nanometers.

Solvents	Toluene	THF	DCM	DMSO	H_2O

	(33.9) [a]	(37.4) [a]	(40.7)	(45.1) [a]	(53.7) [a]
λ_{max}^{abs}	355	361	362	363	365
λ_{max}^{flu}	416	420	426	433	437

[a] Numbers in the first brackets represent the micro-polarity values [E_T (30)] [2] of the solvents. $\lambda_{exc.}$ = 350 nm.

Table S2. Absorption spectra in the UV-visible range and photoluminescence data of compound D were measured in different media and expressed in nanometers.

Solvents	Toluene (33.9) [a]	THF (37.4) [a]	DCM (40.7)	DMSO (45.1) [a]	H_2O (53.7) [a]
λ_{max}^{abs}	358	360	362	363	364
λ_{max}^{flu}	416	419	427	433	437

[a] Numbers in the first brackets represent the micro-polarity values [E_T (30)] [2] of the solvents. $\lambda_{exc.}$ = 350 nm.

Table S3: Determination of ΔG values at various temperatures.

Temperature(℃)	**ΔG (J mol^{-1})**
15	-27418
25	-28370
35	-29322
45	-30274
55	-31226
65	-32178

Table S4: Comparison with the detection limits of sensing Hg^{2+} ions by various sensors

Sl. No	Sensor	Solvent	Sensor type	LOD	LOQ	Portability & cost-effectivity	Application	Ref.
1	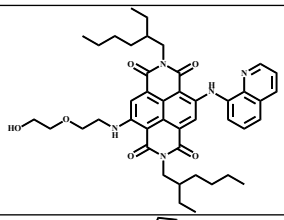	Acetone	Turn-on	3×10^3 nM	10×10^3 nM	YES	NA	3
2	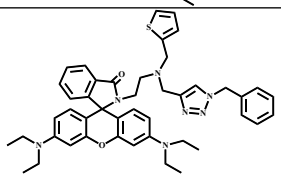	ACN	Turn-on	16 nM	53.3 nM	NA	Metal ion sensor and real sample analysis	4
3	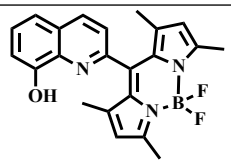	dioxane-water (1:3, v/v) solvent	Turn-off	5×10^3 nM	16.6×10^3 nM	NA	Metal ion sensor	5
4	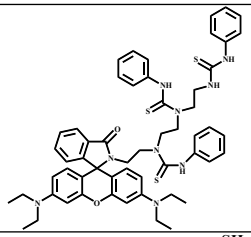	MeCN–HEPES (9 : 1, v/v) medium	Turn-on	30×10^3 nM	100×10^3 nM	NA	Water sample analysis	6
5	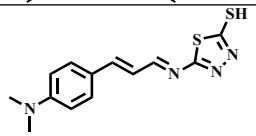	1:1 (v/v) acetonitrile/HEPES Buffer (10mM, pH 7.4)	Turn-on	2×10^3 nM	6.66×10^3 nM	NA	Water sample	7
6	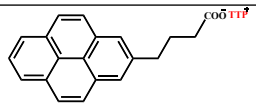	THF	Turn-off	17 nM	56.66 nM	YES	Real sample analysis	8
7	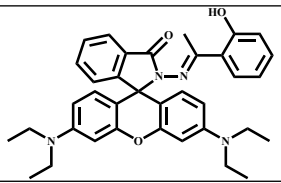	EtOH–water (2 : 1, v/v)	Turn-on	150 nM	500 nM	NA	NA	9
8	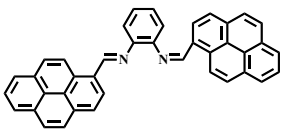	aqueous MeCN	Turn-off	90 nM	300 nM	YES	Paper-test strip application	10

9	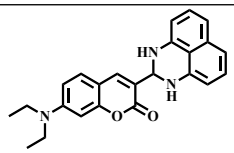	CH_3CN/ H_2O (v/v = 3/7) solutions	Turn-on	1.08× 10^3 nM	3.60× 10^3 nM	NA	Bioimaging in living cells and zebrafish	[11]
10	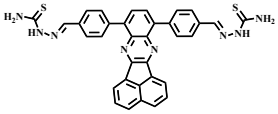	DMSO/ H_2O (v/v=9/1) buffered by 50mMTris-HCl at pH=7.0.	Turn-off	0.90× 10^3 nM	3×10^3 nM	YES	Water sample	[12]
11	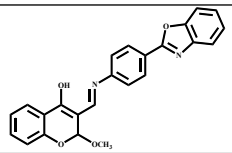	50% (1:1, v/v) H_2O/DMSO	Turn-on	0.40×10^3 nM	1.33× 10^3 nM	YES	Real sample analysis	[13]
12	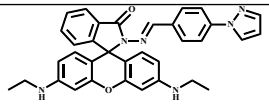	DMSO–water (1 : 1, v/v)	Turn-on	20.70 nM	69 nM	YES	Water sample analysis	[14]
13	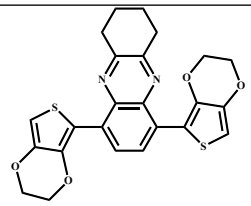 Molecular Weight: 464.56	Mixture of THF and water	Turn-off	17.20× 10^3 nM	56.76 ×10^3 nM	YES	Paper-based sensor	[15]
14	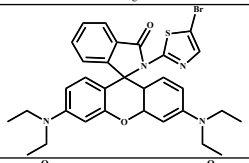	MeCN/H_2O (8:2 v/v)	Turn-on	6.90× 10^3 nM	23× 10^3 nM	NA	Real-time monitoring	[16]
15	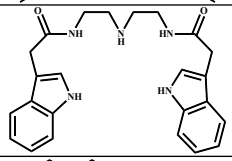	H_2O: EtOH=7: 1, v/v	Turn-off	22.50× 10^3 nM	75× 10^3 nM	NA	NA	[17]
16	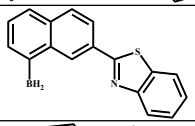	Dioxane-H_2O (9:1, v/v)	Turn-off	30×10^3 nM	100× 10^3 nM	NA	NA	[18]
17	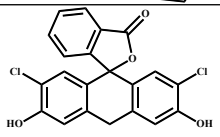	Acetate buffer aqueous 10% DMSO	Turn-off	15×10^3 nM	50× 10^3 nM	NA	NA	[19]
18	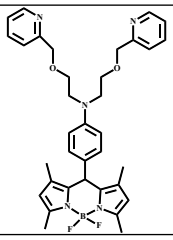	CH_3CN-H_2O (1:1)	Turn-on	18.10× 10^3 nM	60.33 ×10^3 nM	YES	NA	[20]

19	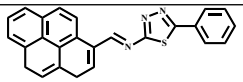	Buffer-CH_3CN (3:7, v/v, 10 mM, pH=7.4)	Turn-on	36 nM	120 nM	YES	NA	[21]
20	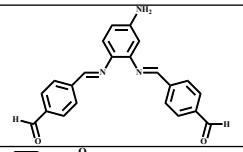	H_2O (pH= 7.4)	Turn-off	0.06×10^3 nM	0.20×10^3 nM	YES	NA	[22]
21	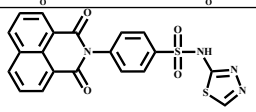	DMSO-Water (1:99, v/v, HEPES buffer pH=7.2	Ratio-metric	14.70 nM	49 nM	NA	NA	[23]
22	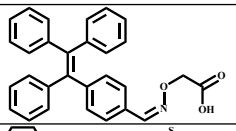	Ethanol-water (3:7)	Ratio-metric	45.40 nM	151.33 nM	NA	Real sample analysis	[24]
23	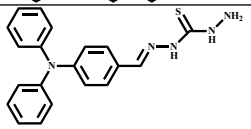	DMSO/Tris-HCl (8:2, v/v, pH=7.0)	Turn-off	31 nM	103.33 nM	YES	Real sample analysis	[25]
24	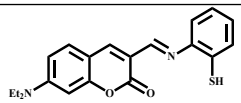	HEPES buffer (20 mM, 3:7 CH_3CN/ H_2O)	Turn-off	50 nM	166.67 nM	YES	Solid sensor	[26]
25	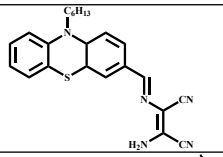	Ethanol-water (6:4, v/v)	Turn-off	17.80 nM	59.33 nM	NA	NA	[27]
26	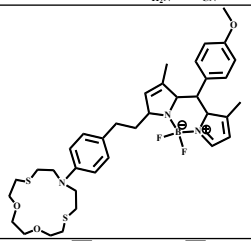	CH_3CN-H_2O (5:95, v/v)	Turn-on	145×10^3 nM	478×10^3 nM	NA	NA	[28]
27	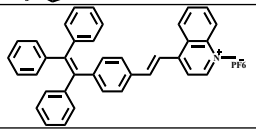	Aqueous (1% DMSO)	Turn-on	591.90 nM	1.90×10^3 nM	NA	NA	[29]

28	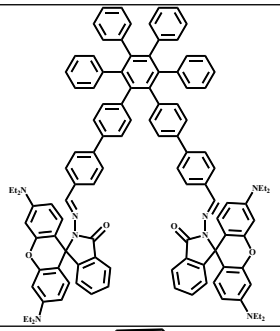	MeCN-water (1 : 1, v/v)	Turn-on	100 nM	0.33× 10^3 nM	NA	NA	[30]
29	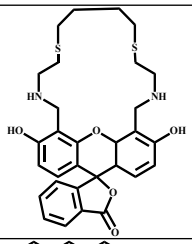	MeOH-Tris-HCl (95:5, v/v, pH=7.2)	Turn-off	7.38 nM	24.60 nM	NA	NA	[31]
30	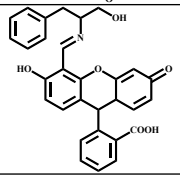	Aqueous medium	Turn-off	0.34× 10^3 nM	1.13× 10^3 nM	YES	Real-time sensing	[32]
31	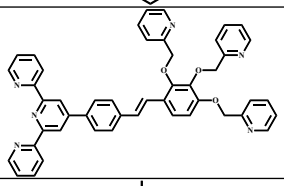	Aqueous medium	Ratio-metric	0.19× 10^3 nM	0.63× 10^3 nM	YES	Real sample analysis	[33]
32	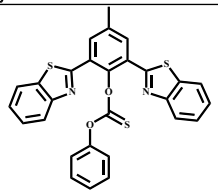	EtOH–water (5/5, v/v, HEPES pH = 7.4)	Turn-on	55 nM	183.30 nM	NA	NA	[34]
33	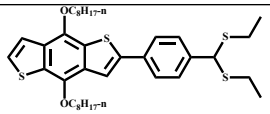	THF–water (1 : 1, v/v)	Ratio-metric	0.31× 10^3 nM	1.03× 10^3 nM	NA	NA	[35]
34	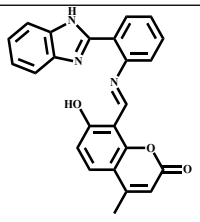	HEPES buffer/DMSO (v/v = 9 : 1, pH = 7.2)	Turn-on	70 nM	0.23× 10^3 nM	NA	biological systems	[36]
35	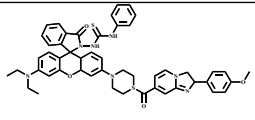	PBS/EtOH (9 : 1, v/v) medium	Turn-on	9.10 nM	30.33 nM	NA	Real sample analysis	[37]
36	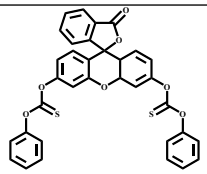	HEPES buffer solution (20 mM, pH 7.4, 1%	Turn-on	40 nM	133.30 nM	NA	NA	[38]

		EtOH)						
37	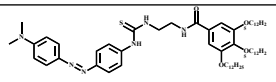	ACN	Colori-metric	9.22 nM	30.73 nM	NA	Multiple metal sensors	[39]
38	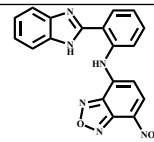	methanol-water (1 : 1) mixture	Colori-metric	47×10^3 nM	156.66×10^3 nM	YES	Real sample analysis	[40]
39	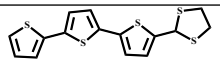	EtOH–water (1 : 1, v/v)	Turn-on	10.3 nM	34.33×10^3 nM	YES	Real sample analysis	[41]
40	**nBTNP**	**100% water**	**Shifting and turn-on**	**9.6 nM**	**31.68 nM**	**YES**	**Real sample analysis**	**This work**

References

1 J. N. Demas and G. A. Crosby, Measurement of photoluminescence quantum yields. Review, *J. Phys. Chem.*, 1971, **75**, 991–1024.

2 C. Reichardt, Solvatochromic dyes as solvent polarity indicators, *Chem. Rev.*, 1994, **94**, 2319–2358.

3 L. Zong, C. Wang, Y. Song, Y. Xie, P. Zhang, Q. Peng, Q. Li and Z. Li, A dual-function probe based on naphthalene diimide for fluorescent recognition of Hg^{2+} and colorimetric detection of Cu^{2+}, *Sensors Actuators B Chem.*, 2017, **252**, 1105–1111.

4 J. Hu, X. Yu, X. Zhang, C. Jing, T. Liu, X. Hu, S. Lu, K. Uvdal, H. W. Gao, and Z. Hu, Rapid detection of mercury (II) ions and water content by a new rhodamine B-based fluorescent chemosensor, *Spectrochim. Acta Part A Mol. Biomol. Spectrosc.*, 2020, **241**, 118657.

5 S. Y. Moon, N. R. Cha, Y. H. Kim and S. K. Chang, New Hg^{2+}-Selective Chromo- and Fluoroionophore Based upon 8-Hydroxyquinoline, *J. Org. Chem.*, 2004, **69**, 181–183.

6 M. Hong, S. Lu, F. Lv, and D. Xu, A novel facilely prepared rhodamine-based Hg^{2+}

fluorescent probe with three thiourea receptors, *Dye. Pigment*, 2016, **127**, 94–99.

7 R. Singh and G. Das, Fluorogenic detection of Hg^{2+} and Ag^{+} ions via two mechanistically discrete signal genres: A paradigm of differentially responsive metal ion sensing, *Sensors Actuators B Chem.*, 2018, **258**, 478–483.

8 N. Tohora, R. Sahoo, S. Ahamed, J. Chourasia, S. Lama, M. Mahato, S. Ali, and S. Kumar Das, Hg(II) causes photoluminescence quenching of pyrene inside a blue-emitting ionic liquid-derived crystalline nanoball, *Phys. Chem. Chem. Phys.*, 2025, **27**, 9478–9490.

9 M. Ozdemir, A rhodamine-based colorimetric and fluorescent probe for dual sensing of Cu^{2+} and Hg^{2+} ions, *J. Photochem. Photobiol. A Chem.*, 2016, **318**, 7–13.

10 Chethanakumar, M. Budri, K. B. Gudasi, R. S. Vadavi and S. S. Bhat, Luminescent Pyrene-based Schiff base Receptor for Hazardous Mercury(II) Detection Demonstrated by Cell Imaging and Test Strip, *J. Fluoresc.*, 2023, **33**, 539–551.

11 C. G. Chen, N. Vijay, N. Thirumalaivasan, S. Velmathi, and S. P. Wu, Coumarin-based Hg^{2+} fluorescent probe: Fluorescence turn-on detection for Hg^{2+} bioimaging in living cells and zebrafish, *Spectrochim. Acta Part A Mol. Biomol. Spectrosc.*, 2019, **219**, 135–140.

12 L. Feng, W. Shi, J. Ma, Y. Chen, F. Kui, Y. Hui and Z. Xie, A novel thiosemicarbazone Schiff base derivative with aggregation-induced emission enhancement characteristics and its application in Hg^{2+} detection, *Sensors Actuators B Chem.*, 2016, **237**, 563–569.

13 T. Sultana, M. Mahato, S. Ahamed, N. Tohora, J. Chourasia, S. Ghanta, and S. Kumar Das, A ‘Turn-on’ fluorogenic probe for selective and specific detection of Hg(II) ions, *J. Photochem. Photobiol. A Chem.*, 2025, **459**, 116028.

14 G. Yang, X. Meng, S. Fang, H. Duan, L. Wang and Z. Wang, A highly selective

colorimetric fluorescent probe for detection of Hg^{2+} and its application on test strips, *RSC Adv.*, 2019, **9**, 8529–8536.

15 E. G. C. Ergun, Three-in-one sensor: a fluorometric, colorimetric and paper-based probe for the selective detection of mercury(II), *New J. Chem.*, 2021, **45**, 4202–4209.

16 T. Rasheed, F. Nabeel, M. Bilal, Y. Zhao, M. Adeel, H. M. N. Iqbal, T. Rasheed, F. Nabeel, M. Bilal, Y. Zhao, M. Adeel, and H. M. N. Iqbal, Aqueous monitoring of toxic mercury through a rhodamine-based fluorescent sensor, *Math. Biosci. Eng. 2019 41861*, 2019, **16**, 1861–1873.

17 H. H. Wu, Y. L. Sun, C. F. Wan, S. T. Yang, S. J. Chen, C. H. Hu, and A. T. Wu, Highly selective and sensitive fluorescent chemosensor for Hg^{2+} in aqueous solution, *Tetrahedron Lett.*, 2012, **53**, 1169–1172.

18 Y. H. Kim, S. Y. Jin, Y. M. So, J. I. Choe, and S. K. Chang, Hg^{2+}-selective Fluorogenic Chemosensor Derived from 8-Aminoquinoline, *Chem. Lett.*, 2004, **33**, 702–703.

19 M. G. Choi, H. De Ryu, H. L. Jeon, S. Cha, J. Cho, H. H. Joo, K. S. Hong, C. Lee, S. Ann, and S. K. Chang, Chemodosimetric Hg^{2+}-selective signaling by mercuration of dichlorofluorescein derivatives, *Org. Lett.*, 2008, **10**, 3717–3720.

20 A. Maity, A. Sil, S. Nad and S. K. Patra, A highly selective, sensitive and reusable BODIPY based ‘OFF/ON' fluorescence chemosensor for the detection of Hg^{2+} Ions, *Sensors Actuators B Chem.*, 2018, **255**, 299–308.

21 C. B. Bai, P. Xu, J. Zhang, R. Qiao, M. Y. Chen, M. Y. Mei, B. Wei, C. Wang, L. Zhang, and S. S. Chen, Long-Wavelength Fluorescent Chemosensors for Hg^{2+} based on Pyrene, *ACS Omega*, 2019, **4**, 14621–14625.

22 A. Kumar, R. Ananthakrishnan, G. Jana, P. K. Chattaraj, S. Nayak and S. K. Ghosh, An Intramolecular Charge Transfer Induced Fluorescent Chemosensor for Selective

Detection of Mercury (II) and its Self-Turn-On Inside Live Cells at Physiological pH, *ChemistrySelect*, 2019, **4**, 4810–4819.

23 B. Muzey and A. Naseem, An AIEE active 1, 8-naphthalimide- sulfamethizole probe for ratiometric fluorescent detection of Hg^{2+} ions in aqueous media, *J. Photochem. Photobiol. A Chem.*, 2020, **391**, 112354.

24 Y. Yuan, X. Chen, Q. Chen, G. Jiang, H. Wang, and J. Wang, New switch on fluorescent probe with AIE characteristics for selective and reversible detection of mercury ion in aqueous solution, *Anal. Biochem.*, 2019, **585**, 113403.

25 Y. Li, W. Shi, J. Ma, X. Wang, X. Kong, Y. Zhang, L. Feng, Y. Hui, and Z. Xie, A novel optical probe for Hg^{2+} in aqueous media based on mono-thiosemicarbazone Schiff base, *J. Photochem. Photobiol. A Chem.*, 2017, **338**, 1–7.

26 Shaily, A. Kumar and N. Ahmed, Indirect Approach for CN- Detection: Development of 'naked-Eye' Hg^{2+}-Induced Turn-Off Fluorescence and Turn-On Cyanide Sensing by the Hg^{2+} Displacement Approach, *Ind. Eng. Chem. Res.*, 2017, **56**, 6358–6368.

27 K. M. Vengaian, C. D. Britto, K. Sekar, G. Sivaraman and S. Singaravadivel, Phenothiazine-diaminomalenonitrile based Colorimetric and Fluorescence "Turn-off-on" Sensing of Hg^{2+} and S^{2-}, *Sensors Actuators B Chem.*, 2016, **235**, 232–240.

28 M. Lo Presti, R. Martínez-Máñez, J. V. Ros-Lis, R. M. F. Batista, S. P. G. Costa, M. M. Raposo and F. Sancenón, A dual channel sulphur-containing a macrocycle functionalised BODIPY probe for the detection of Hg(II) in a mixed aqueous solution, *New J. Chem.*, 2018, **42**, 7863–7868.

29 R. X. Zhang, P. F. Li, W. J. Zhang, N. Li and N. Zhao, A highly sensitive fluorescent sensor with aggregation-induced emission characteristics for the detection of iodide and mercury ions in aqueous solution, *J. Mater. Chem. C*, 2016, **4**, 10479–10485.

30 G. Singh, S. I. Reja, V. Bhalla, D. Kaur, P. Kaur, S. Arora and M. Kumar,

Hexaphenylbenzene appended AIEE active FRET based fluorescent probe for selective imaging of Hg^{2+} ions in MCF-7 cell lines, *Sensors Actuators B Chem.*, 2017, **249**, 311–320.

31 P. Piyanuch, S. Watpathomsub, V. S. Lee, H. A. Nienaber and N. Wanichacheva, Highly sensitive and selective Hg^{2+}-chemosensor based on dithia-cyclic fluorescein for optical and visual-eye detections in aqueous buffer solution, *Sensors Actuators B Chem.*, 2016, **224**, 201–208.

32 R. V. Rathod, S. Bera, P. Maity and D. Mondal, Mechanochemical Synthesis of a Fluorescein-Based Sensor for the Selective Detection and Removal of Hg^{2+} Ions in Industrial Effluents, *ACS Omega*, 2020, **5**, 4982–4990.

33 J. Wang, Q. Rao, H. Wang, Q. Zhang, G. Liu, Z. Wu, J. Yu, X. Zhu, Y. Tian, and H. Zhou, A terpyridine-based test strip for the detection of Hg^{2+} in various water samples and drinks, *Anal. Methods*, 2019, **11**, 227–231.

34 J. Xu, Z. Xu, Z. Wang, C. Liu, B. Zhu, X. Wang, K. Wang, J. Wang, and G. Sang, A carbonothioate-based highly selective fluorescent probe with a large Stokes shift for detection of Hg^{2+}, *Luminescence*, 2018, **33**, 219–224.

35 T. Leng, Y. Ma and G. Chen, A novel ratiometric fluorescence and colorimetric probe with a large Stokes shift for Hg2+ sensing, *J. Photochem. Photobiol. A Chem.*, 2018, **353**, 143–149.

36 Y. Gao, C. Zhang, S. Peng and H. Chen, A fluorescent and colorimetric probe enables simultaneous differential detection of Hg^{2+} and Cu^{2+} by two different mechanisms, *Sensors Actuators B Chem.*, 2017, **238**, 455–461.

37 Y. Li, S. Qi, C. Xia, Y. Xu, G. Duan, and Y. Ge, A FRET ratiometric fluorescent probe for detection of Hg2+ based on an imidazo[1,2-a]pyridine-rhodamine system, *Anal. Chim. Acta*, 2019, **1077**, 243–248.

38 A. Picard-Lafond, D. Larivière and D. Boudreau, Revealing the Hydrolysis Mechanism of a Hg^{2+}-Reactive Fluorescein Probe: Novel Insights on Thionocarbonated Dyes, *ACS Omega*, 2020, **5**, 701–711.

39 X. Cao, Y. Li, Y. Yu, S. Fu, A. Gao and X. Chang, Multifunctional supramolecular self-assembly system for colorimetric detection of Hg^{2+}, Fe^{3+}, $Cu^{2+,}$ and continuous sensing of volatile acids and organic amine gases, *Nanoscale*, 2019, **11**, 10911–10920.

40 T. Anand and S. K. Sahoo, Cost-effective approach to detect Cu(II) and Hg(II) by integrating a smartphone with the colorimetric response from a NBD-benzimidazole based dyad, *Phys. Chem. Chem. Phys.*, 2019, **21**, 11839–11845.

41 L. Lan, Q. Niu and T. Li, A highly selective colorimetric and ratiometric fluorescent probe for instantaneous sensing of Hg^{2+} in water, soil, and seafood and its application on test strips, *Anal. Chim. Acta*, 2018, **1023**, 105–114.